Tibi, R., Wiens, D. A., Yuan, X. (2008): Seismic evidence for widespread serpentinized forearc mantle along the Mariana convergence margin. - Geophysical Research Letters, 35, L13303

DOI: 10.1029/2008GL034163.

Seismic Evidence for Widespread Serpentinized Forearc Mantle Along the Mariana Convergence Margin

Rigobert Tibi[1], Douglas A. Wiens[1], and Xiaohui Yuan[2]

[1] Department of Earth and Planetary Sciences, Washington University,
St. Louis, Missouri 63130, USA
email: tibi@wustl.edu

[2] GeoForschungsZentrum Potsdam, 14473 Potsdam, Germany

Submitted *Geophysical Research Letters*, March 28, 2008

Revised May 22, 2008

Abstract

Seismic imaging of subduction zones can provide constraints on mineral reactions in the slab and surrounding regions. We use *P*-to-*S* converted phases from teleseisms recorded at broadband stations in the Mariana Islands to image the forearc and arc regions of the Mariana convergent margin. The subducting oceanic crust is observed between 75 and 110 km depth as a thin low velocity zone overlying the subducting Moho, demonstrating that the basalt to eclogite phase transition must occur at a greater depth. A low velocity zone (LVZ), approximately 10–25 km thick, whose upper boundary is imaged at about 40–55 km depth, is detected in the forearc region of the mantle wedge along the entire margin. The anomaly is located too shallow to represent subducted oceanic crust. We interpret the LVZ as a serpentinized region in the forearc mantle, resulting from hydration by slab-expelled water. The inferred *S*-wave velocity in the LVZ of as low as ~3.6 km/s represents a level of serpentinization of 30–50%, corresponding to a chemically bound water content of about 4–6 wt%.

1. Introduction

Fluids are a critical ingredient for a variety of processes occurring in subduction zones. For instance, slab-derived fluids are thought to promote partial melting in the warm part of the overlying mantle wedge, causing magmatism. In the cold forearc region of the mantle wedge, hydration of mantle peridotite by slab-expelled fluids may lead to serpentinization [e.g., *Peacock,* 1990]. Thermal models for subduction zones predict temperatures of about 100–600°C in the forearc mantle, with the lower values of the range expected to occur in island arcs with thin forearc crust such as the Izu-Bonin and Mariana arcs [*Hyndman and Peacock,* 2003]. Antigorite, a high-temperature mineral of the serpentine group, is stable to temperatures of about 600–700°C [*Ulmer and Trommdorff,* 1995]. Hence, it is expected to be stable in the cold forearc mantle of these convergence margins. Seismic evidence for serpentinization of the forearc mantle has been observed in several subduction zones, including Japan, Central Andes, Cascadia, Izu-Bonin, Middle America [*Kamiya and Kobayashi*, 2000; *Graeber and Asch*, 1999; *Bostock et al.*, 2002; *Kaminura et al.*, 2002; *DeShon and Schwartz*, 2004]. In each case, serpentinization in the mantle wedge has been identified from the detection of unusually low velocities and/or, more importantly, high Poisson's ratios.

The forearc region of the Mariana margin contains numerous active serpentinite mud volcanoes [e.g., *Fryer*, 1996]. Samples collected from these volcanoes show evidence for slab-derived fluids [*Fryer et al.*, 1999], clearly suggesting that forearc hydration is occurring there. Despite this compelling geochemical evidence, however, a strong seismic argument for subduction-related serpentinization of the Mariana forearc has yet to be reported. In this study, we use *P*-to-*S* converted waves from teleseisms recorded in the

Mariana Islands and show evidence for widespread serpentinazation of the forearc mantle along this margin.

2. Data and Analysis

We applied the *P*-wave receiver function methodology [e.g., *Kind et al.*, 1995; *Yuan et al.*, 1997] using teleseisms from 241 earthquakes with m_b 5.4 or greater, recorded at a temporary network of broadband stations on the Mariana Islands. The network consisted of 20 IRIS-PASSCAL stations and the Global Seismic Network station GUMO located in the island of Guam (Fig. 1). The former instruments operated from May 2003 to May 2004 as part of the MARGINS Subduction Factory Experiment of the Mariana system [*Tibi et al.*, 2006]. For the permanent station GUMO, we used data recorded in the time period of 1991 to 2005.

Seismograms from earthquakes at epicentral distances between 30° and 95° are deconvolved to ground displacement and filtered at 2–30 sec. The waveforms are rotated from the ZNE recording system into an LQT ray coordinate system. A source equalization scheme is applied by deconvolving the *P* energy on the L component from the rotated traces. The resulting Q and T components are termed Q and T receiver functions (RF's), respectively. For a horizontally layered, isotopic medium, there should be no converted energy on the tangential (T) component. Presence of energy on this component is diagnostic of heterogeneity or anisotropy.

P-to-*S* conversions are low-amplitude phases hardly visible in individual RF's. In order to enhance these phases, the RF's are stacked along their moveout curve. Prior to stacking, RF's from different epicentral distances are moveout-corrected for primary

conversion *Ps* using a reference distance of 67°. For the moveout-correction, we use a modified IASP91 velocity model [*Kennett and Engdahl*, 1991]. The modification includes a crustal *P* velocity model for the Mariana arc obtained from an active-source study [*Takahashi et al.*, 2007]. The crustal *S* velocities were derived from that model assuming V_P/V_S of 1.73. To constrain the average 1-D *S*-wave velocity structure beneath the stations, traces resulting from stacked Q component RF's are inverted using the approach described by *Kind et al.* [1995].

3. Results and Discussion

Fig. 2A,B shows the first 20 sec after *P* onset of moveout-corrected and stacked Q and T component RF's, respectively, for stations on the islands of Tinian and Saipan. Four coherent phases appear in the stacked Q traces (Fig. 2A). (1) The large, positive phase immediately after 0 sec results from interference between converted energy from shallow interfaces. (2) The negative phase at about 4–6 sec delay time, observed between the longitude range of 145.6–146.1°E, represents a *Ps* conversion from an interface at about 50 km depth. Fig. 2B shows that no significant *SH* energy is associated with this feature, consistent with a subhorizontal interface and predominantly isotropic layer above it. This is in agreement with shear wave splitting measurements, which show small average splitting times in the upper 80–100 km for the region [*Pozgay et al.*, 2007]. (3) A positive phase, which can be correlated between the longitude range of 145.3–145.7°E at ~10–11 sec delay time, is preceded ~1.4 sec earlier by (4) a negative phase (Fig. 2A). The timings of both the negative and positive phases seem to be consistent with shallowly westward-dipping interfaces. The presence of corresponding significant *SH* energy on the transverse

traces unequivocally supports this view (Fig. 2B). On the transverse traces, the two phases can be correlated throughout the sampled longitude range from 145.3 to 146.1°E. As discussed below, we interpreted these phases as being conversions from the top of the subducting low velocity Pacific crust and Pacific Moho, respectively.

3.1 Nature of the 50-km Interface

Sufficient data were recorded by the nine stations located on the islands of Tinian and Saipan, allowing generation of migrated sections of RF's [*Kind et al.*, 2002]. Fig. 2C shows the result of the migration procedure for an east-west section along AB profile. The location of the profile is indicated in Fig. 1. The 50-km interface undulates between about 40 and 55 km depth, and is observed only east of 145.6°E. We could not infer the easternmost extent of this feature, as the available data do not sample it beyond about 146°E (Fig. 2C). Ocean bottom seismographs deployed in the northern part of the arc do not produce clean RF's due to reverberations in the water layer, and thus do not allow examination of the outer forearc.

The 50-km interface, which we observe beneath all the stations along the Mariana margin (Fig. 3A), is restricted to the forearc region, sampled mostly by earthquakes from the Tonga subduction zone. A subset of data composed only of non-Tonga events sampling the forearc shows the 50-km interface too, suggesting that this feature is not associated with a near-source structure in the Tonga region. The interface is not an artifact associated with a particular ray parameter and back-azimuth, as it is imaged throughout a range of these parameters. The 50-km interface does not represent a discontinuity directly related to the subducting plate, such as the top of the slab, for two reasons. (1) Unlike the top of the

slab, which is dipping westward, the 50-km interface is subhorizontal. (2) And, more importantly, there are areas where both the 50-km interface and the top of the subducted plate are imaged as two distinct features, with the former lying ~30 km above the latter (Fig. 2C). The restriction of the 50-km interface to the forearc region suggests that a process, which is taking place exclusively in the forearc mantle, is the likely cause for this feature. Considering all these characteristics, we interpret the 50-km interface as marking the upper boundary of a LVZ that extends down to immediately above the descending Pacific plate. We believe that the LVZ represents a region in the forearc mantle hydrated (serpentinized) by slab-expelled fluids. Serpentinization of the forearc mantle causes the velocity there to decrease. The negative conversion associated with the top side of the LVZ is consistent with that, and indicates that velocity in the LVZ has become slower than that in the region above it. We do not image the lower boundary of the serpentinized region, which would show a velocity increase with depth, probably because the low-velocity subducting crust bounds this region downward. The presence of the low-velocity crust reduces the velocity contrast across that boundary making it invisible in the data.

In order to constrain the structure of the serpentinized zone, Q component RF's sampling predominantly the forearc were stacked in 1-degree latitude bins of piercing points at 50 km depth. These are traces from events with back-azimuth from 0 to 180°. The stacked RF's for each bin were subsequently inverted for average *S*-wave velocities. The inversions reveal both the upper and lower boundaries of the serpentinized zone. Results suggest that, for the longitude range sampled by the data, the thickness of the serpentinized zone varies from ~10 km beneath Rota, Tinian and Saipan in the southern region of the margin to ~25 km beneath Guguan, Alamagan and Pagan in the northern

region (Fig. 3A, bottom). The occurrence of the serpentinized zone along the entire margin suggests that serpentinization of the forearc mantle is a widespread phenomenon in the Mariana arc. *S*-wave velocities in the serpentinized zone are estimated to be as low as ~3.6 km/s. *S*-wave velocities alone cannot rule out other possible causes for the observed anomaly. Provided our proposition is correct and following *Christensen* [1966] and *Carlson and Miller* [2003], the estimated lower bound of *S*-wave velocity within the serpentinized zone represents a degree of serpentinization as high as 30–50% for the Mariana forearc mantle. This corresponds to bound water content of about 4–6 wt%. A similarly high level of serpentinization of the forearc mantle wedge has been inferred for the Cascadia margin [*Bostock et al.*, 2002]. Serpentinization of the Mariana forearc mantle is evidenced by the occurrence in the forearc of numerous mud volcanoes, composed mainly of unconsolidated flows containing clasts of serpentinized mantle peridotite [*Fryer*, 1996; *Fryer et al.*, 1999].

Beneath Tinian and Saipan, the western boundary of the serpentinized region in the mantle wedge is located ~40 km east of the volcanic front (Fig. 2C), and most likely corresponds to the point beyond which arcward temperatures are too hot for serpentine to be stable. Data limited to records from island stations does not allow us to constrain the eastward extent of the serpentinized zone. However, presence of serpentine seamounts within about 50 km from the trench axis [*Fryer et al.*, 1985] suggests that serpentinization of the mantle wedge by slab-derived fluids is occurring across most of the entire forearc to that location. Serpentine in the near-trench region may lubricate the plate interface, reducing the seismogenic width for shallow thrust earthquakes. This provides an

164 explanation for the near-complete absence of large shallow thrust events in the Mariana
165 margin.
166
167 **3.2 The Subducting Crust**
168 Using Q component RF's, both the top and bottom side of the subducting crust are
169 imaged as gently westward-dipping interfaces in the longitude range between about 145.3
170 and 145.8°E beneath Tinian and Saipan (Fig. 2C). In this longitude range, the interfaces
171 are sampled predominantly updip, generating strong *Ps* phases. Trenchward beyond
172 145.8°E, however, most of the rays are incident on the slab in the downdip direction,
173 resulting in weak, mostly invisible conversions from the subducting crust, consistent with
174 ray-theoretical predictions [e.g., *Cassidy,* 1992]. The dipping Pacific plate deflects waves
175 from the Q-L plane, thus generating slab energy on T component. Migrated T component
176 RF's clearly show both the top and bottom side of the subducting crust throughout the
177 range from 145.3 to 146.1°E (Fig. 2D). In this longitude range, the bottom of the
178 subducting crust (Pacific Moho) is observed between 75 and 110 km depth. Observation of
179 the Pacific Moho at 110 km depth, suggests that at that depth, the subducting crust is still a
180 low-velocity channel that has not yet eclogitized. Otherwise there would be little or no
181 impedance contrast to the surrounding mantle [*Helffrich et al.*, 1989; *Hacker et al.*, 2003].
182 To constrain the velocity in the subducting crust, Q component RF's from events in
183 the back-azimuth range from 180 to 360° were stacked in 1-degree latitude bins of piercing
184 points at 100 km depth, and subsequently inverted. Most of these events sample the
185 backarc region. Because their rays are incident in the updip direction of the slab, these
186 events should generate clear conversion from slab interfaces. Both the top and bottom side

of the subducting crust are observed only beneath the region extending from Rota to Saipan (Fig. 3B, top). The fact that the slab is not continuously imaged along the margin may be indicative of along-strike variability in eclogitization. Fig. 3B, bottom displays inversion results for the two stacks showing conversion from slab interfaces. In the inversions, we took into account the dip of the subducting crust by adjusting the incidence angle for the theoretical traces in relation to the dip angle of the downgoing Pacific place. The subducting crust beneath Rota, Tinian and Saipan is modeled as a 12–15 km low velocity layer with a reduction of *S*-wave velocity of ~10% relative to the surrounding mantle (Fig. 3B, bottom). Unlike the thickness, which probably may have been overestimated by the inversion procedure, the inferred velocity reduction in the subducting crust is well within the range of 5–15% observed in other arcs [*Helffrich and Abers*, 1997; *Abers*, 2000; *Yuan et al.*, 2000], and consistent with mineral physics compilations [*Hacker et al.*, 2003].

Acknowledgments

Portable seismic equipment was provided by PASSCAL program of IRIS. We would like to thank James Conder for discussions on the thermal structure of Mariana mantle wedge, and Patrick Shore, Juan Camacho, Sara Pozgay, Allan Sauter, and Brian Shiro for deploying the stations. We are grateful to Tom Brocher for his comments on the manuscript. This research was financially supported by NSF under grants OCE0001938 and EAR0310272.

References

Abers, G. A. (2000), Hydrated subducted crust at 100–250 km depth, *Earth Planet. Sci Lett., 176*, 323-330.

Bostock, M. G., R. D. Hyndman, S. Rondenay, and S. M. Peacock (2002), An inverted continental Moho and serpentinization of the forearc mantle, *Nature, 417*, 536-538.

Carlson, R. L., and J. D. Miller (2003), Mantle wedge water contents estimated from seismic velocities in partially serpentinized peridotites, *Geophys. Res. Lett., 30*, 1250, doi: 10.1029/2002GL016600.

Cassidy, J. F. (1992), Numerical experiments in broadband receiver function analysis, *Bull. Seismol. Soc. Am., 82*, 1453-1474.

Christensen, N. I. (1966), Elasticity of ultrabasic rocks, *J. Geophys. Res., 71*, 5921-5931.

DeShon, H. R., and S. Y. Schwartz (2004), Evidence for serpentinization of the forearc mantle wedge along the Nicoya Peninsula, Costa Rica, *Geophys. Res. Lett., 31*, L21611, doi: 10.1029/2004GL021179.

Fryer, P. (1996), Evolution of the Mariana convergent plate margin system, *Rev. Geophys., 34*, 89-125.

Fryer, P., E. L. Ambos, and D. M. Husong (1985), Origin and emplacement of Mariana forearc seamounts, *Geology, 13*, 774-777.

Fryer, P., C. G. Wheat, and M. J. Mottl (1999), Mariana blueschist mud volcanism: Implications for conditions within the subduction zone, *Geology, 27*, 103-106.

Graeber, F. M., and G. Asch (1999), Three-dimensional models of *P* wave velocity and *P*-to-*S* velocity ratio in the southern central Andes by simultaneous inversion of local earthquake data, *J. Geophys. Res. 104*, 20,237-20,256.

232 Gudmundsson, Ó., and M. Sambridge (1998), A regionalized upper mantle (RUM) seismic
233 model, *J. Geophys. Res., 103*, 7121-7136.
234 Hacker, B. R., G. A. Abers, and S. M. Peacock (2003), Subduction factory, 1, Theoretical
235 mineralogy, densities, seismic wave speeds, and H_2O contents, *J. Geophys. Res.*,
236 *108*, 2029, doi: 10.1029/2001JB001127.
237 Helffrich, G., and G. A. Abers (1997), Slab low-velocity layer in the eastern Aleutian
238 subduction zone, *Geophys. J. Int., 130*, 640-648.
239 Helffrich, G. R., S. Stein, and B. J. Wood (1989), Subduction zone thermal structure and
240 mineralogy and their relationship to seismic wave reflections and conversions at the
241 slab/mantle interface, *J. Geophys. Res., 94*, 753-763.
242 Hyndman, R. D., and S. M. Peacock (2003), Serpentinization of the forearc mantle, *Earth*
243 *Planet. Sci. Lett., 212*, 417-432.
244 Kamimura, A., J. Kasahara, M. Shinohara, R. Hino, H. Shiobar., G. Fujie, and T.
245 Kanazawa (2002), Crustal structure study at the Izu-Bonin subduction zone around
246 31°N: Implications of serpentinized materials along the subduction plate boundary,
247 *Phys. Earth Planet. Inter., 132*, 105-129.
248 Kamiya, S., and Y. Kobayashi (2000), Seismological evidence for the existence of
249 serpentinized wedge mantle, *Geophys. Res. Lett., 27*, 819-822.
250 Kennett, B. L. N., and E. R. Engdahl (1991), Traveltimes for global earthquake location
251 and phase identification, *Geophys. J. Int., 105*, 429-465.
252 Kind, R., G. L. Kosarev, and N. V. Petersen (1995), Receiver functions of the stations of
253 the German Regional Seismic Network (GRSN), *Geophys. J Int., 121*, 191-202.

Kind, R., X. Yuan, J. Saul, D. Nelson, S. V. Sobolev, J. Mechie., W. Zhao, G. Kosarev, J. Ni, U. Achauer, and M. Jiang (2002), Seismic images of crust and upper mantle beneath Tibet: Evidence for Eurasian plate subduction, *Science, 298*, 1219-1221.

Peacock, S. M. (1990), Fluid processes in subduction zones, *Science, 248*, 329-337.

Pozgay, S. H., D. A. Wiens, J. A. Conder, H. Shiobara, and H. Sugioka (2007), Complex mantle flow in the Mariana subduction system: Evidence from shear wave splitting, *Geophys. J. Int., 170*, 371-386.

Takahashi, N., S. Kodaira, S. L. Kemplerer, Y. Tatsumi, Y. Kaneda, and K. Suyehiro (2007), Crustal structure and evolution of the Mariana intra-oceanic island arc, *Geology, 35*, 203-206.

Tibi, R., D. A. Wiens, H. Shiobara, H. Sugioka, and P. J. Shore (2006), Depth of the 660-km discontinuity near the Mariana slab from an array of ocean bottom seismographs, *Geophys. Res. Lett., 33*, L02313, doi: 10.1029/2005GL024523.

Ulmer, P., and V. Trommsdorf (1995), Serpentine stability to mantle depths and subduction-related magmatism, *Science, 268*, 858-861.

Yuan, X., J. Ni, R. Kind, J. Mechie, and E. Sandvol (1997), Lithospheric and upper mantle structure of southern Tibet from a seismological passive source experiment, *J. Geophys. Res., 102*, 27,491-27,500.

Yuan et al. (2000), Subduction and collision processes in the Central Andes constrained by converted seismic phases, *Nature, 408*, 958-961.

Figure Captions

Figure 1. Bathymetric map of the Mariana region. Triangles indicate the locations of PASSCAL broadband seismic stations, and square the location of the GSN station GUMO. Gray lines are contours of seismicity [*Gudmundsson and Sambridge*, 1998], and numbers indicate depth in km to the seismogenic zone. Dots are locations of the ray-theoretical *Ps* piercing points at 100 km depth for the calculated RF's. Line A-B indicates the location of the profiles shown in Figure 2C and D. Inset at the upper-left corner shows the locations of the earthquakes used in this study (circles) and the Mariana network (triangle).

Figure 2. (A) Stacked Q component RF's recorded at nine stations on the islands of Tinian and Saipan. The traces have been averaged over longitude bins of 0.1°, and sorted in order of increasing mean longitude of *Ps* piercing points at 100 km depth. The longitude scale is only valid for that depth. The number of RF's stacked for each bin is indicated in the box. Positive and negative phases are shown in red and blue, respectively. Yellow circles mark conversions from the upper boundary of the serpentinized zone. Green and black circles mark conversions from the top and bottom side of the subducted crust, respectively. (B) The same as in (A) but for T component RF's. Note that there is no *SH* energy associated with the upper boundary of the serpentinized zone (see text). (C) East-west profile of migrated Q component receiver function data. The location of the profile is shown in Figure 1. Red (blue) indicates velocity increase (decrease) downward. Yellow dashed line marks the upper boundary of the serpentinized zone. Green and black dashed lines mark the top and bottom side of the subducted crust, respectively. Multiple reverberations from

297 the upper boundary of the serpentinized zone are labeled ‘multiples’. VF stands for
298 volcanic front. (D) The same as in (C) but for T component data.
299
300 **Figure 3.** (A) (Top) Stacked Q component RF’s from events in the back-azimuth range
301 between 0 and 180°. The traces have been averaged over latitude bins of 1°, and sorted in
302 order of increasing mean latitude of *Ps* piercing points at 50 km depth. The number of
303 RF’s stacked for each bin is indicated in the box. Yellow circles indicate conversions from
304 the upper boundary of the serpentinized zone. (Bottom) 1-D *S*-wave velocity model for
305 each latitude bin obtained after inversion of the traces displayed on the top. Red arrows
306 mark the upper and lower boundary of the serpentinized region (SR), indicated in purple.
307 Black arrows mark the bottom side of the subducted crust (SC). Fits of theoretical RF’s
308 (red) to the observed data (black) are shown below each model panel. The 50-sec long
309 waveforms include direct conversions (*Ps*) and multiple reververations (*PpPs* and *PpSs* +
310 *PsPs*) from the upper boundary of the serpentinized zone. (B) (Top) The same as in (A)
311 (top) but for events in the back-azimuth range between 180 and 360°, and the latitude of *Ps*
312 piercing points at 100 km depth. The gray rectangle highlights conversions from the top
313 (green circles) and bottom side (black circles) of the subducted crust beneath the region
314 extending from Rota to Saipan. (Bottom) 1-D velocity model for the two latitude bins
315 showing clear conversions from the subducted crust (top). Green and black arrows mark
316 the top and bottom side of the subducted crust (SC), respectively. Fits of theoretical RF’s
317 (red) to the observed data (black) are shown below each model panel.

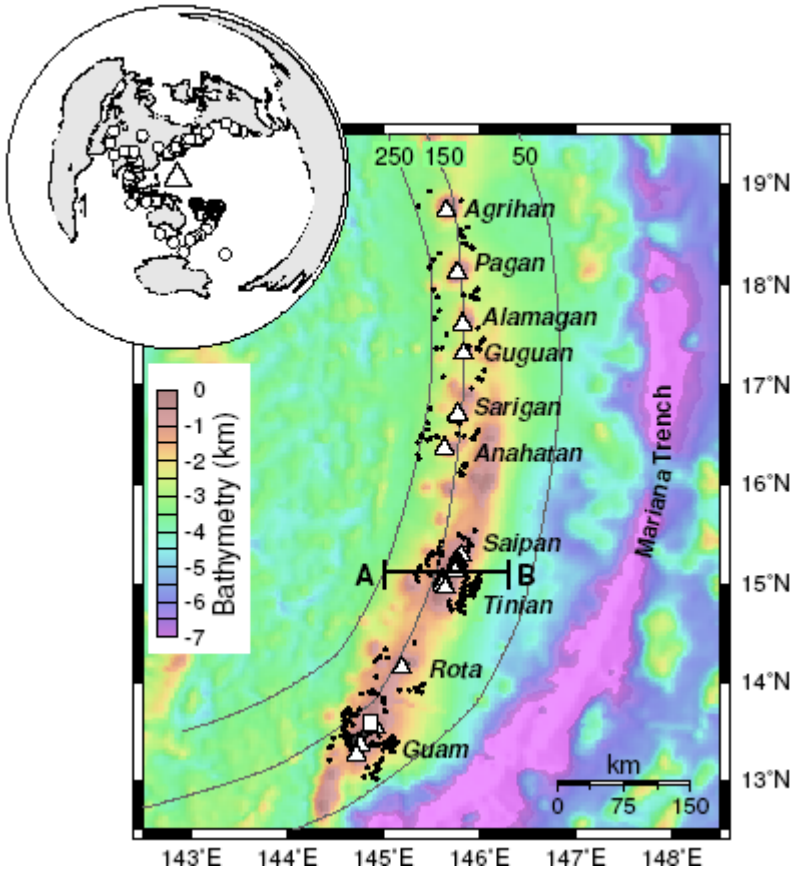

Figure 1: Tibi et al.

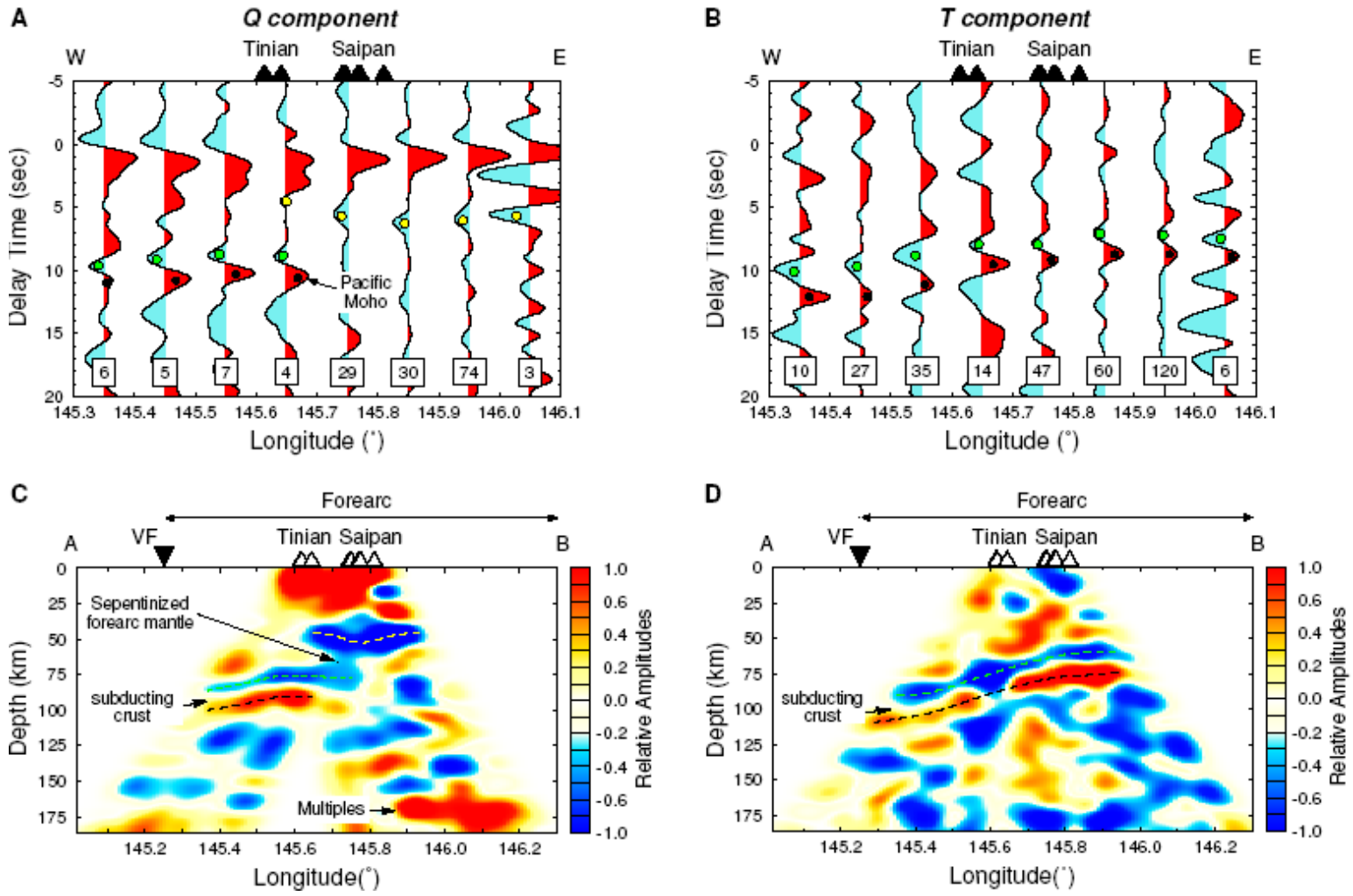

Figure 2: Tibi et al.

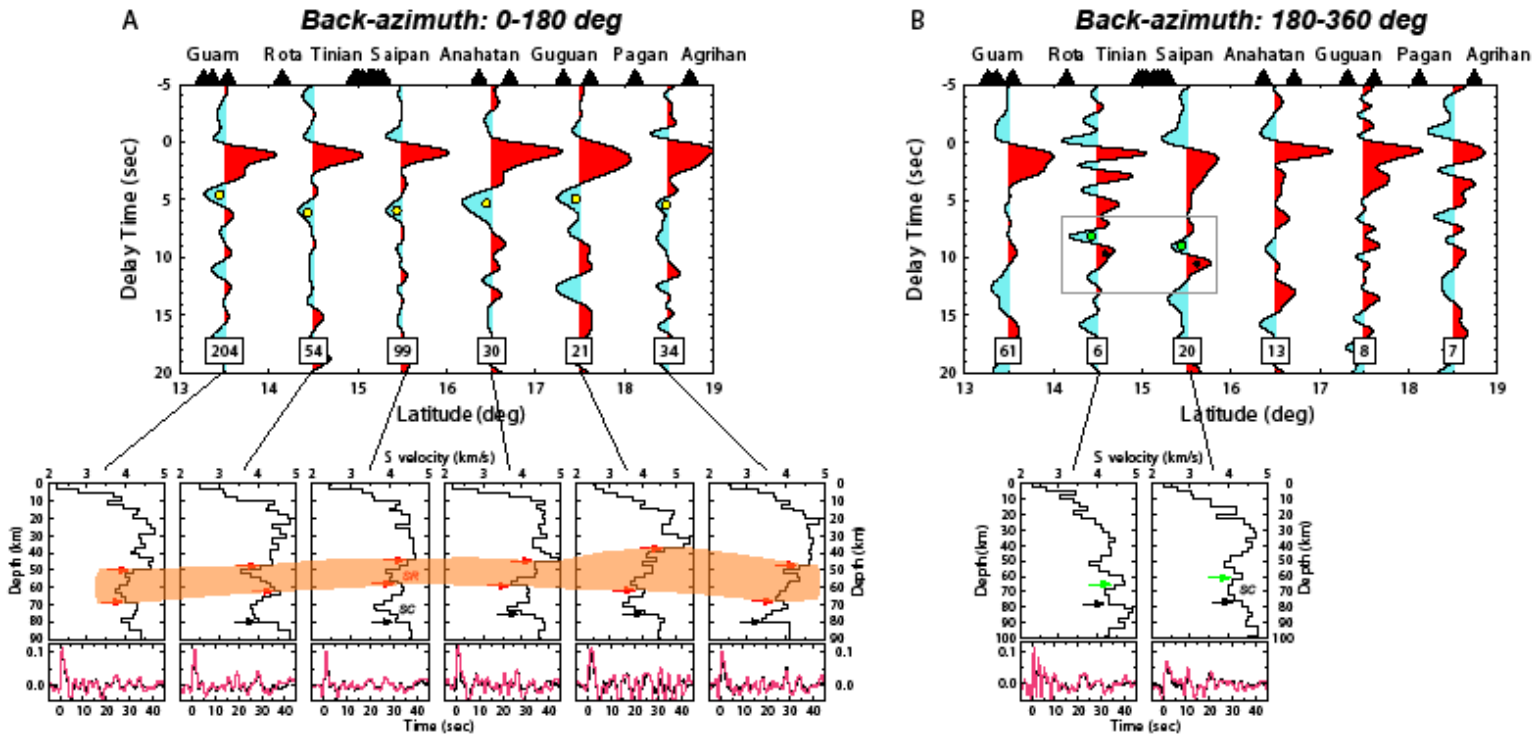

Figure 3: Tibi et al.